Numerical simulation of the pairwise interaction of deformable cells during migration in a microchannel

Hongzhi Lan and Damir B. Khismatullin*
Department of Biomedical Engineering, Tulane University, New Orleans, Louisiana 70118, USA
(Received 25 August 2013; revised manuscript received 24 May 2014; published 21 July 2014)

Leukocytes and other circulating cells deform and move relatively to the channel flow in the lateral and translational directions. Their migratory property is important in immune response, hemostasis, cancer progression, delivery of nutrients, and microfluidic technologies such as cell separation and enrichment, and flow cytometry. Using our three-dimensional computational algorithm for multiphase viscoelastic flow, we have investigated the effect of pairwise interaction on the lateral and translational migration of circulating cells in a microchannel. The numerical simulation data show that when two cells with the same size and small separation distance interact, repulsive interaction take place until they reach the same lateral equilibrium position. During this process, they undergo swapping or passing, depending on the initial separation distance between each other. The threshold value of this distance increases with cell deformation, indicating that the cells experiencing larger deformation are more likely to swap. When a series of closely spaced cells with the same size are considered, they generally undergo damped oscillation in both lateral and translational directions until they reach equilibrium positions where they become evenly distributed in the flow direction (self-assembly phenomenon). A series of cells with a large lateral separation distance could collide repeatedly with each other, eventually crossing the centerline and entering the other side of the channel. For a series of cells with different deformability, more deformable cells, upon impact with less deformable cells, move to an equilibrium position closer to the centerline. The results of our study show that the bulk deformation of circulating cells plays a key role in their migration in a microchannel.

DOI: 10.1103/PhysRevE.90.012705 PACS number(s): 87.85.gf, 47.61.Jd, 47.57.ef, 87.85.M−

I. INTRODUCTION

Circulating cells, including blood cells such as erythrocytes (red blood cells), thrombocytes (platelets), and leukocytes (white blood cells), and other individual cells under certain conditions (e.g., tumor cells during hematogenous metastasis [1]), are deformable and drastically different in their geometric and mechanical properties [2]. Circulating cells move in a channel relatively to the external flow in the lateral (transverse) and translational directions. This migratory property of circulating cells plays a crucial role in immune response, hemostasis, cancer progression, and delivery of nutrients [1,3–6], and has been proposed to be used for flow cytometry and cell separation and enrichment in microfluidic devices [7–12]. Most microfluidic methods for cell separation require the external assistance of fluorescence, magnetic force, electrophoresis, and/or optical trapping [13]. However, it is possible to separate or enrich circulating cells by a purely hydrodynamic approach [14–19]. This method, known as inertial microfluidics, is based on the fact that a deformable particle migrates to a specific lateral position in a microchannel depending on its size and deformability [15,20].

Much research on the migration of circulating cells and deformable particles in flow channels was conducted in the simplest scenario of negligible intercellular or interparticle interactions where the cell-to-cell or particle-to-particle distance was much larger than the size of the cells or particles. In this scenario, which we call *scenario A*, the lateral migration of a single particle in a confined channel is driven by the shear force and wall repulsion that lead the particle to a specific lateral equilibrium position, either at the centerline or between the centerline and the wall [21–26]. With lateral lift force, both deformable particles and cells migrate to midway between the centerline and the wall of a channel [15,20]. A number of mathematical models were proposed as well to investigate scenario A [27–35]. These models predicted that a bigger or more deformable particle or cell had the lateral equilibrium position closer to the centerline, which was consistent with experimental data.

However, scenario A does not work for dense suspension flow in a microchannel because of the large volume fraction of circulating cells and thus a close spacing between cells [36]. In the scenario of dense suspension, called *scenario B*, the migration of circulating cells significantly depends on hydrodynamic cell-cell interactions. Hydrodynamic interactions between erythrocytes and leukocytes and between erythrocytes and thrombocytes were studied in a number of experimental works [3–6,37,38]. These studies revealed that the geometric (size, shape) and mechanical properties (deformability) of the cells contribute to the increased concentration of erythrocytes near the centerline and leukocyte and thrombocyte margination [39]. Erythrocyte accumulation near the centerline leads to the formation of a thin cell-free layer adjacent to the capillary wall. This layer is responsible for the Fahraeus effect, i.e., a decrease in tube hematocrit and apparent viscosity of the blood with a decrease in the capillary diameter [40]. Leukocyte margination, i.e., their lateral migration to vessel wall margins, is necessary for leukocytes to adhere to the wall and initiate the immune response [4]. Similarly, the migration of thrombocytes to vessel wall margins is a necessary step in blood clotting [41]. In terms of microfluidic applications for scenario B, it is important to mention biomimetic separation of leukocytes during whole blood perfusion in a microfluidic channel [9].

*damir@tulane.edu

Lattice Boltzmann, immersed boundary, and boundary integral methods have been used to model the flow of a dense suspension of deformable particles or cells in a microchannel [42–47]. The results of these computational studies indicate that highly deformable particles or erythrocytes concentrate near the centerline during circulation, which pushes out solid particles, leukocytes, or thrombocytes from the centerline to the channel wall. The shape difference between cells was also considered in numerical studies as different types of cells have different morphologies, such as a spherical shape for leukocytes, a biconcave shape for erythrocytes, and an ellipsoidlike or oblate shape for platelets [39]. The nonspherical shape of erythrocytes was shown to be essential for their concentration at the centerline of the channel and for leukocyte margination [43,48].

There exists another scenario (*scenario AB*) where the interactions between particles or cells may be significant but the average separation distance is larger than in the case of a dense suspension (scenario B). One example is the "single chain" flow of particles or cells in a small channel where a moving particle or cell interacts with only two neighbors located at some distance from the cell [49]. This self-assembly of circulating particles or cells has been employed in biomedicine, material synthesis, and logical computation [50–52] and shown to be very important for microfluidics-based flow cytometry and cell separation [53,54]. Recent experimental studies show that circulating particles migrate to a specific lateral position where they are uniformly spaced in the flow direction (like beads on a string) as a result of the balance of attractive and repulsive interactions between nearby particles [49,55–57]. The analysis of scenario AB is very important for optimization of microfluidic technologies for cell separation and enrichment because of the potential to increase the efficiency of cell separation when the cell concentration or volume fraction is between that of the dense and dilute suspensions. The pairwise interactions of spherical and nonspherical rigid particles in linear or quadratic shear flows have already been investigated [49,58–60]. It was theoretically established that the flow disturbances induced by a rotating particle could repel the neighboring particle with only fluid inertia maintaining a finite distance between the particles [49]. The interactions of two deformable particles have not been analyzed in the context of cell migration in confined channels. Previous work focused on the interaction of two elastic solid particles close to the wall in linear shear flow [61] and the effect of the collision of two elastic capsules or drops on their deformation in linear shear flow [62–65].

As much research has been carried out on the simulation of dense suspension of erythrocytes, our focus in this study is on circulating leukocyte dynamics in a microfluidic channel under scenario AB. Using our volume-of-fluid (VOF) computational algorithm, we have investigated how the pairwise interactions of circulating cells influence their lateral and translational migration during perfusion through a microchannel. Our fully three-dimensional (3D) numerical simulation of scenario AB was performed for cells of different deformability and initial distribution in the microchannel.

II. NUMERICAL ALGORITHM

Our computational model is based on a fully three-dimensional algorithm for multiphase viscoelastic flow, where the fluid-fluid interface is tracked by the volume-of-fluid (VOF) method [34,66,67]. The external fluid is a Newtonian fluid with viscosity $\mu_{\text{ext}} = 1$ cP (water). The cell is modeled as a one-phase complex fluid with two internal compartments: a solvent (cytosol) and a polymer matrix (cytoskeleton). We assume that the solvent viscosity μ_s is equal to the viscosity of the external fluid. The viscoelasticity of the polymer matrix is described by the Giesekus constitutive equation [66]:

$$\lambda\left(\frac{\partial \mathbf{T}}{\partial t} + (\mathbf{u}\cdot\nabla)\mathbf{T} - (\nabla\mathbf{u})\mathbf{T} - \mathbf{T}(\nabla\mathbf{u})^T\right) + \mathbf{T} + \lambda\kappa\mathbf{T}^2 = \lambda G(0)(\nabla\mathbf{u} + (\nabla\mathbf{u})^T). \quad (1)$$

Here κ is the Giesekus nonlinear parameter and was assumed to be zero in the current study, $G(0)$ the elastic modulus at $t = 0$, and λ the relaxation time. The polymer viscosity is $\mu_p = G(0)\lambda$. The total viscosity of the cell is $\mu_d = \mu_s + \mu_p$.

The velocity field in the whole computational domain was determined from the solution of one set of the Navier-Stokes equations with the values of physical parameters (mass density, shear viscosity, etc.) averaged over each grid cell containing multiple phases [66]:

$$\nabla\cdot\mathbf{u} = 0, \quad (2)$$

$$\rho\left(\frac{\partial \mathbf{u}}{\partial t} + \mathbf{u}\cdot\nabla\mathbf{u}\right) = \nabla\cdot\mathbf{T} - \nabla p + \nabla\cdot[\mu_s(\nabla\mathbf{u} + (\nabla\mathbf{u})^T)] + \mathbf{F}. \quad (3)$$

Here, $\mathbf{u}$ is the velocity vector, ρ the mass density, $\mathbf{T}$ the extra stress tensor that represents the polymer matrix (cytoskeleton) contribution to the shear stress field inside the cell, and p pressure. The interfacial tension force $\mathbf{F}$ (known as cortical tension for the cell) is calculated by the continuous surface force (CSF) method [68] as follows:

$$\mathbf{F} = \sigma\tilde{\kappa}||\nabla c||\hat{\mathbf{n}}, \quad (4)$$

where σ is the cortical tension coefficient, $\hat{\mathbf{n}} = \nabla c/||\nabla c||$ the outward unit normal, $\tilde{\kappa} = -\nabla\cdot\hat{\mathbf{n}}$ the mean curvature, $c = c(t,\mathbf{x})$ the concentration function (color function) that takes the value between 0 and 1 at the interface, and $\mathbf{x} = (x, y, z)$ the position vector in the Cartesian coordinate system. To simplify the problem, we assume that the mass density of the external fluid and the cell are equal and gravity is ignored.

In the simulation, we consider two cells of initially spherical shape with the same diameter D suspended at the middle plane ($y = W/2$) of a rectangular microchannel with height $H = 70$ μm and width $W = 140$ μm (Fig. 1). All the side walls of the microchannel are considered to be no-slip boundaries, and periodic boundary conditions are applied at the inlet and outlet. Initially, the flow is fully established with the centerline velocity U_c, with a range of values from 0.014 to 0.70 m/s. In most cases studied, $U_c = 0.14$ m/s, which is based on the flow conditions in microfluidic experiments by Hur *et al.* [15]. We consider the cells with diameter $D = 14$ μm; elastic modulus $G(0) = 12.5$, 25, 50, and 250 Pa; relaxation time $\lambda = 0.2$ s; and cortical tension coefficient $\sigma = 0.03$ mN/m. These values were selected according to the experimental data for human leukocytes [2,66,69,70]. It should be noted that with our choice of the elastic modulus values,

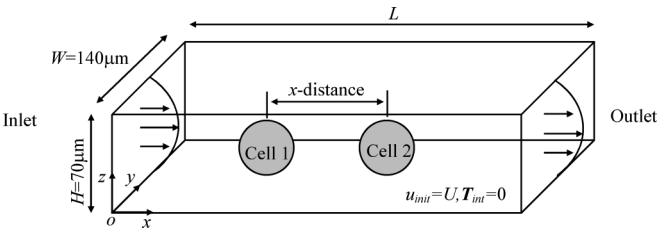

FIG. 1. Schematic of the simulated problem. Two interacting cells in a rectangular microchannel. The cells may have different deformability and different spacing in the x direction (translational direction) and/or the z direction (lateral direction). They are subject to shear flow created by a pressure difference between inlet and outlet. Periodic boundary conditions have been applied at the inlet and outlet. No-slip boundary conditions were applied to the channel walls in the y and z directions. Chanel height H and width W are 70 and 140 μm, respectively. Channel length L is variable.

the total viscosity of the cell is within the experimental range of 2.5–50 Pa s. The results are presented in dimensionless form using D or H as a characteristic length and $t^* = H/U_c$ as a characteristic time. With the selected values of physical parameters, the channel height–based Reynolds number $\mathrm{Re} = \frac{\rho_{\mathrm{ext}} U_c H}{\mu_{\mathrm{ext}}}$ and the cell-to-external fluid viscosity ratio $\gamma = \frac{\mu_p}{\mu_{\mathrm{ext}}}$ range from 1 to 50 and from 2500 to 10 000, respectively. In most cases, $\mathrm{Re} = 10$ at which the wall shear stress averaged over the channel perimeter is about 6 Pa. Since D/H is 0.2 in all the simulation except the data presented in Fig. 10, the Reynolds number based on the cell diameter is five times less than the channel height–based Reynolds number. Different from erythrocytes, leukocyte migration and deformation are dominated by bulk rheological properties (e.g., viscosity), not by surface rheological properties (e.g., cortical or interfacial tension) [2,34]. As such, the viscosity ratio is a more appropriate measure of cell deformability than the capillary number.

III. RESULTS AND DISCUSSION

We first considered the case of a long channel, 30 times the cell diameter, to eliminate the effects of periodic boundary conditions (and thus cells in domains adjacent to the computational domain) on the interaction of migrating cells. In this simulation, the translational distance between the cell centroids, called the x distance [blue dashed line in Fig. 2(a)], was initially ten times the cell diameter. This ensures that the cell-cell interaction was initially negligible. By changing the initial z distance, i.e., the initial distance between the cell centroids in the lateral direction, we investigated the migration of both cells (cell 1 and cell 2) in a microchannel. With initial z distance$/D = 0.286$, the cells first moved slowly towards the lateral equilibrium position as expected according to our previous study on single cell migration [34]. As their x distance decreased to five times the cell diameter at $t/t^* = 16$, the migration deviated from the trajectory of a single migrating cell and the pairwise interaction became significant. The rate by which the cells approached each other in the lateral direction suddenly increased and then the cell positions were stabilized. The cells never collided and their x distance$/D$ was no less than 3.2. When the cells reached this minimal translational

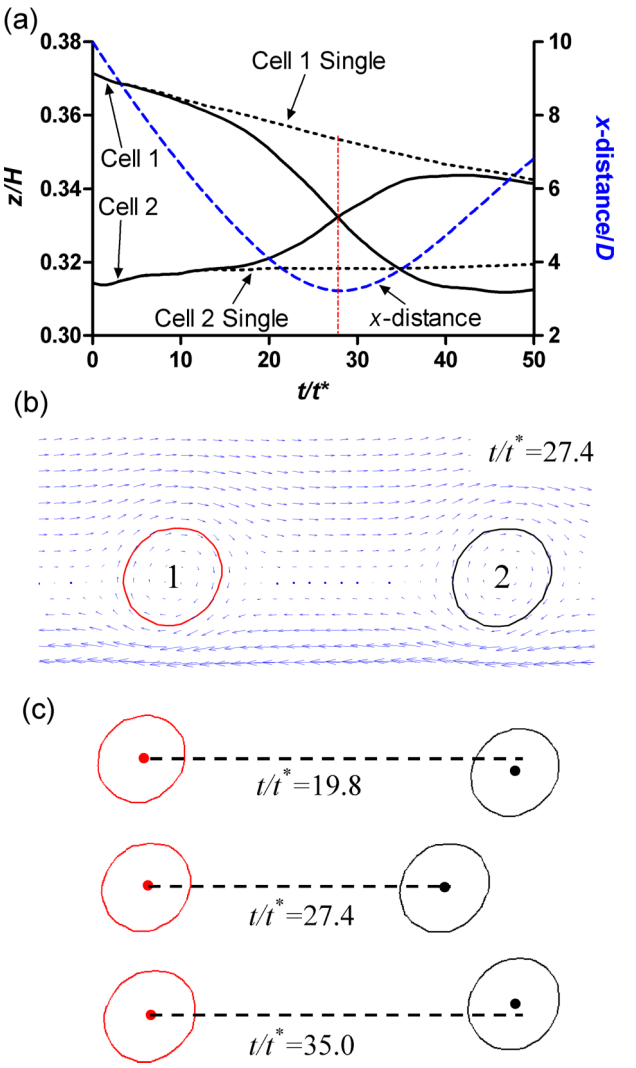

FIG. 2. (Color online) The swapping of two identical cells during migration in a microchannel. (a) Time evolution of the cell lateral positions (solid lines) and cell-to-cell translational distance (x distance$/D$, blue dashed line) when the initial lateral separation distance (z distance$/D$) is 0.286 (initial lateral position z_0/H for cells 1 and 2 is 0.371 and 0.314, respectively). Black dotted lines are the z position of single migrating cells (scenario A). (b) Flow field at $t/t^* = 27.4$ with the center of cell 1 used as a reference point. (c) Snapshots of cell shapes at $t/t^* = 19.8$, 27.4 and 35. Here, the x coordinate of the cell 2 spheroid is calculated relative to that of the cell 1 spheroid. The channel length is $30D$, and the initial translational position x_0/H for cells 1 and 2 is 2.0 and 4.0, respectively. $\mathrm{Re} = 10$, $\gamma = 10^4$, $D/H = 0.2$.

distance (at $t/t^* = 27.4$), they had the same lateral position. After $t/t^* = 27.4$, cell 1 continued to move downward, while cell 2 moved upward. As a result, cell 1 went below cell 2 and cell 2 started moving faster than cell 1, as evident by positive and increasing values of the x distance after $t/t^* = 27.4$ [blue dashed line in Fig. 2(a)]. At $t/t^* = 50$, the x distance$/D$ was 6.8 and the cells migrated like single cells again and eventually reached their lateral equilibrium position, which was higher than the initial z position for cell 2 and much lower than the initial z position for cell 1. This case

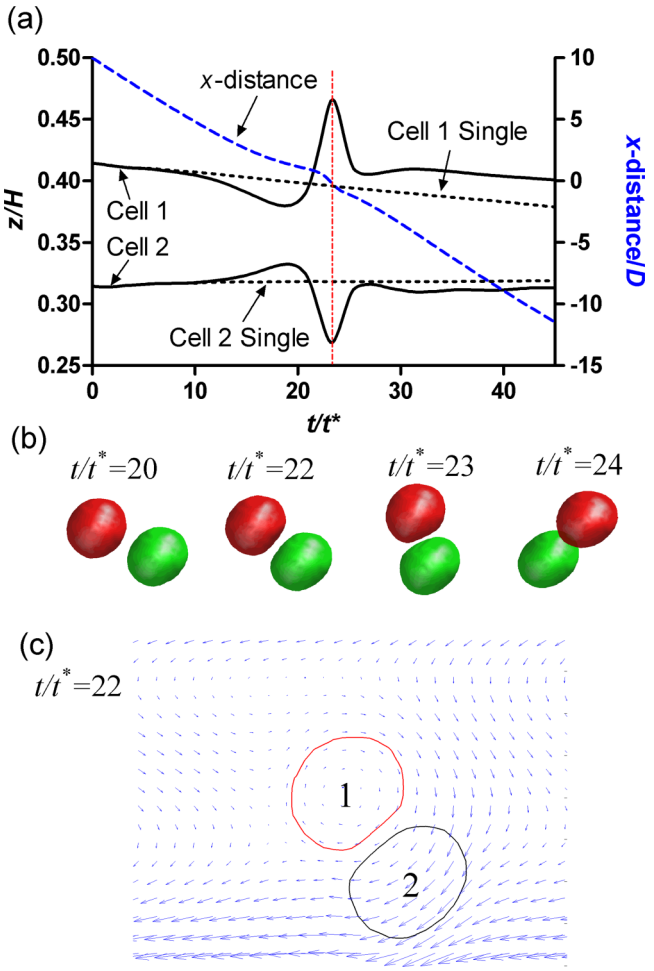

FIG. 3. (Color online) The passing of two identical cells during migration in a microchannel. (a) Time evolution of the lateral positions of the cells (black solid lines) and cell-to-cell x distance (blue dashed line) when the initial z distance/D is 0.5 (z_0/H for cells 1 and 2 is 0.414 and 0.314, respectively). (b) Snapshots of cell shapes at $t/t^* = 20$, 22, 23, and 24. (c) Flow field at $t/t^* = 22$ with the center of cell 1 used as a reference point. The channel length is $30D$; the initial translational position x_0/H for cells 1 and 2 is 2.0 and 4.0, respectively. Re = 10, $\gamma = 10^4$, $D/H = 0.2$.

illustrates that although the cells at the end are far from each other and their position equilibrates, they can be "swapped" during transient interactions occurring before reaching this equilibrium position. Figure 2(b) shows the flow field at $t/t^* = 27.4$ with the centroid of cell 1 as a reference point. The wall reflection of the flow produced by one of the rotating cells drove the other one across the streamline, leading to relative reversal migration in the z direction. This is similar to the simulation data for two particles in simple shear flow [58]. Figure 2(c) displays the shapes of the cells at different time instants. It points out that swapping occurs when the x distance becomes minimal.

With the initial z distance/D increased to 0.5, cell 1 was positioned closer to the centerline and moved faster in the x direction than cell 2 (Fig. 3). This led to a decrease in the x distance with a concurrent decrease in the z distance. Similar to the data in Fig. 2, the cells first moved like single cells until the x distance decreased to five times the cell diameter. Then they started to interact and followed the swapping trajectories in the lateral direction. However, the swapping process stopped prematurely at $t/t^* = 20$, when the cells came close to each other and underwent large deformation. The z distance between the cells suddenly increased and reached to the maximum value at $t/t^* = 23.1$ when the x distance became zero [red dotted line in Fig. 3(a)]. After $t/t^* = 23.1$, cell 1 passed cell 2 (the x distance changed the sign) and the cell-cell interaction weakened. The cells recovered their precollision shapes and moved back rapidly to the lateral position slightly higher (in the case of cell 1) or lower (cell 2) than they had before $t/t^* = 20$. In this case, cell 1 remained closer to the centerline and faster in the translational direction than cell 2, and thus the absolute value of the x distance continued to increase with time and the interaction gradually vanished. The three-dimensional view of the computed cell shape during the above-described passing process is shown in Fig. 3(b). Significant flattening of the cells occurred at the regions where the cell-to-cell separation distance was small. Figure 3(c) shows the flow field at $t/t^* = 22$ with the centroid of cell 1 serving as a reference point.

The numerical simulation of the previous two cases indicates that the trajectories of the cells change from swapping to passing when the initial z distance between the cells increases above a certain threshold value. We investigated the effects of flow rate, cell viscosity, and cell position on the threshold z distance. In this analysis, the z distance was determined at the time when the x distance between the cells becomes five times the cell diameter. This condition was selected based on the data in Figs. 2 and 3 that showed the onset of pairwise interaction at the x distance below or equal to $5D$. As the flow rate increases (Re = 1, 10, 50), the critical z distance/D increases from 0.367 to 0.402 [Fig. 4(a)]. When the cell viscosity increases ($\gamma = 2500$, 5000, 10 000), the critical z distance/D decreases from 0.398 to 0.368 [Fig. 4(b)]. If the positions of the cells become closer to the centerline ($z/H = 0.2$, 0.32, 0.38 for the lower cell), the critical z distance/D decreases from 0.42 to 0.34 [Fig. 4(c)]. These results indicate that when the cells experience larger deformation due to higher flow rate, lower viscosity, or closer proximity to the channel wall, the critical z distance below which the cell swapping occurs increases. Thus, the probability of swapping becomes higher with larger deformation of the cells.

The related problem is how the threshold value of the z distance changes when considering two cells with different bulk viscosities. We ran the simulation where cell 1 (the upper cell) was more deformable than cell 2. The critical z distance/D decreased from 0.398 in the case of identical cells to 0.255 in the case when cell 2 was four times more viscous than cell 1 ($\gamma_1 = 2500$, $\gamma_2 = 10\,000$). This change was much higher than that shown in Fig. 4 for identical cells. This result indicates that if the upper cell is more deformable or the lower cell is less deformable, the probability of cell swapping substantially reduces. This is not the case if the upper cell becomes less deformable than the lower cells. If $\gamma_1 = 10\,000$ and $\gamma_2 = 2500$, the critical z distance/D is 0.468, which is larger than the corresponding values for identical cells in Fig. 4. Both cases show that the pairwise interaction facilitates the migration of more deformable cells towards the

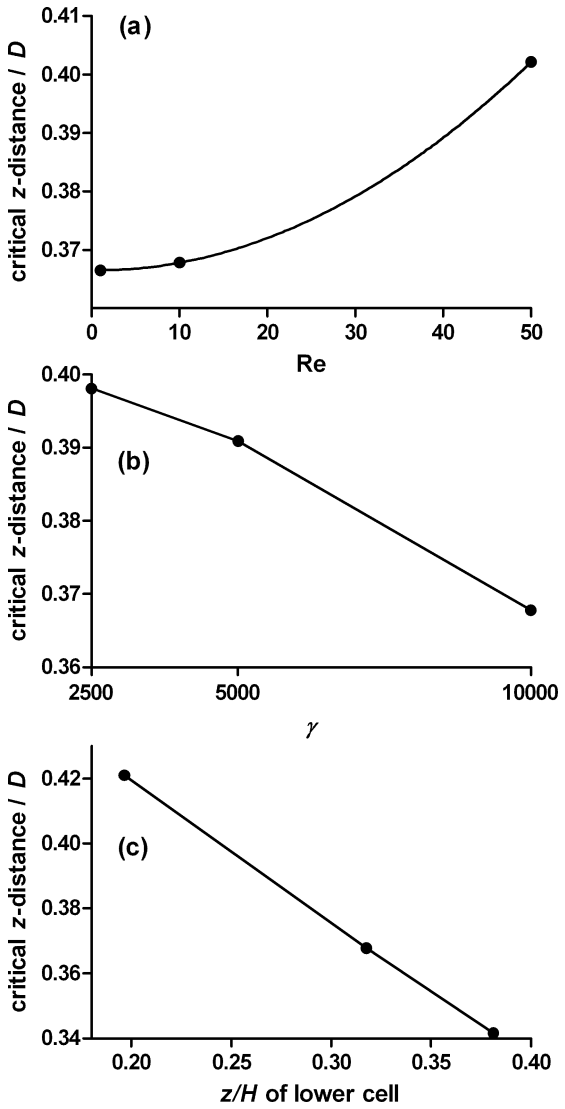

FIG. 4. The effect of flow rate (a), cell viscosity (b) and cell position (c) on the critical z distance of two interacting cells. $D/H = 0.2$. (a) z/H for the lower cell is 0.32, $\gamma = 10^4$. (b) z/H for the lower cell is 0.32, Re $= 10$. (c) $\gamma = 10^4$, Re $= 10$.

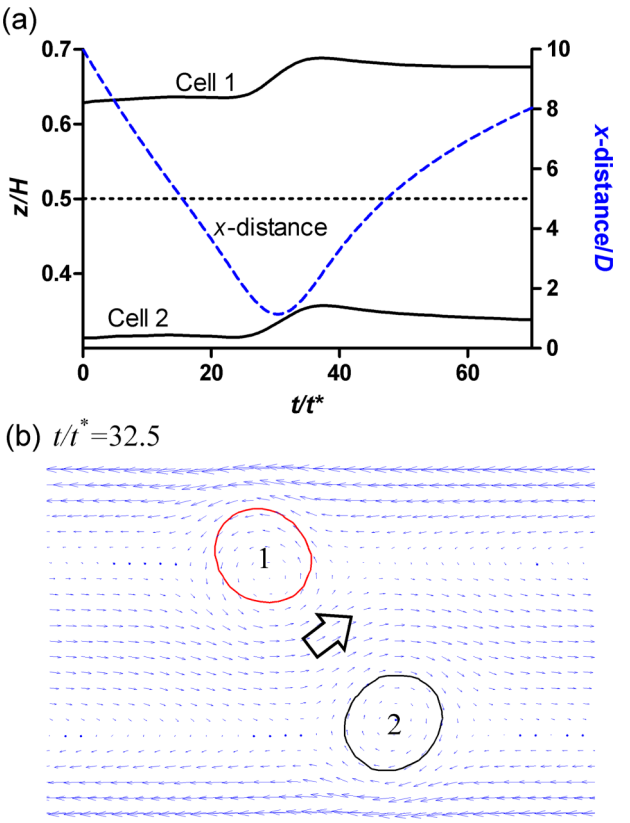

FIG. 5. (Color online) The interaction of two identical cells located in different halves of the microchannel. (a) Time evolution of the cell lateral positions (solid lines) and cell-to-cell x distance (blue dashed line) when z_0/H for cells 1 and 2 is 0.629 and 0.314, respectively. (b) Flow field at $t/t^* = 32.5$ with the centroid of cell 2 used as a reference point. The channel length is $30D$, and the initial translational position x_0/H for cells 1 and 2 is 2.0 and 4.0, respectively. Re $= 10$, $\gamma = 10^4$, $D/H = 0.2$.

centerline. These results also point out that it is important to consider the initial lateral position of cells in a microchannel for deformability-based cell separation. If more deformable cells are positioned at the inlet closer to the centerline than less deformable cells, most of the cells will migrate in the channel without swapping, i.e., the cells will not be mixed and can be efficiently separated at small distances from the channel inlet. However, if more deformable cells are closer to the wall than less deformable cells, they will swap when they migrate. The cells need to travel a sufficiently large distance along the channel for swapping to be completed and the final z distance large enough for separation to be reached. Thus, with less deformable cells positioned closer to the centerline, a long channel is required for efficient deformability-based cell separation.

In all the cases we considered above, both cells were located in the same bottom half of the channel. Figure 5 shows the numerical data on pairwise interaction of cells migrating in different (top and bottom) halves of the channel. One interesting result is that as the cells get closer to each other, their lateral migration occurs synchronously in the same direction, not in the opposite direction as in Figs. 2(a) and 3(a). This phenomenon seems to contradict intuition, but could be explained by the flow field shown in Fig. 5(b) at $t/t^* = 32.5$ when the x distance$/D$ reaches the minimum. The existence of cell 1 introduces a small region of the flow field in the direction marked by a big arrow in Fig. 5(b). The recirculating flow around an upwardly migrating cell 1 lifts cell 2, thereby leading to synchronous motion of two cells.

Here, we consider the pairwise interaction between the cells located in a short channel, where periodic boundary conditions will influence the cell migration. Physically, this case describes the migratory dynamics of a long periodic series of cells [Fig. 6(a)]. Two identical cells were put in with the same initial lateral position z_0 but different translational position x_0. The channel length was ten times the cell diameter and the initial x distance between the cells was three times the cell diameter. As shown in Fig. 6(b), both migrating cells underwent damped oscillation in the lateral direction around the same equilibrium position. These oscillations were in antiphase (i.e., the phase shift was 180°) and had a period of about $51t^*$ and the maximum amplitude of $0.136D$. The distance between the cells

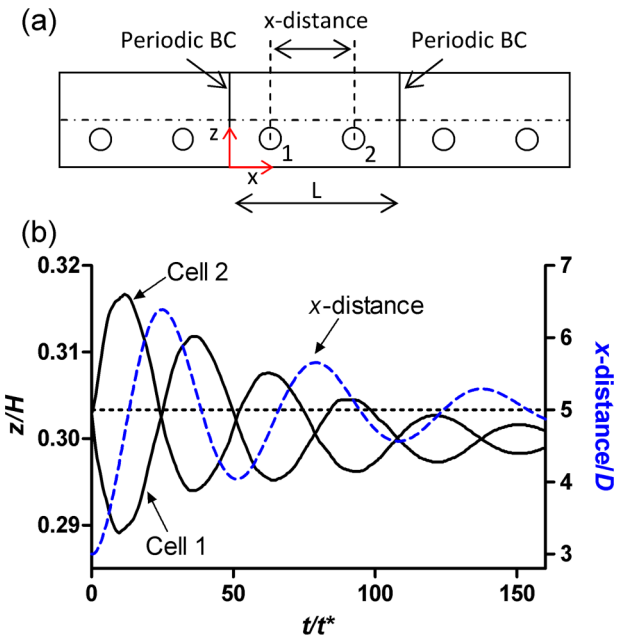

FIG. 6. (Color online) (a) Diagram of a long series of cells located in the same half of the channel. (b) Time evolution of the cell lateral positions (solid lines) and cell-to-cell x distance (blue dashed line) when z_0/H for cells 1 and 2 is 0.303. The channel length is $10D$, and the initial translational position x_0/H for cells 1 and 2 is 0.7 and 1.3, respectively. Re $= 10$, $\gamma = 10^4$, $D/H = 0.2$.

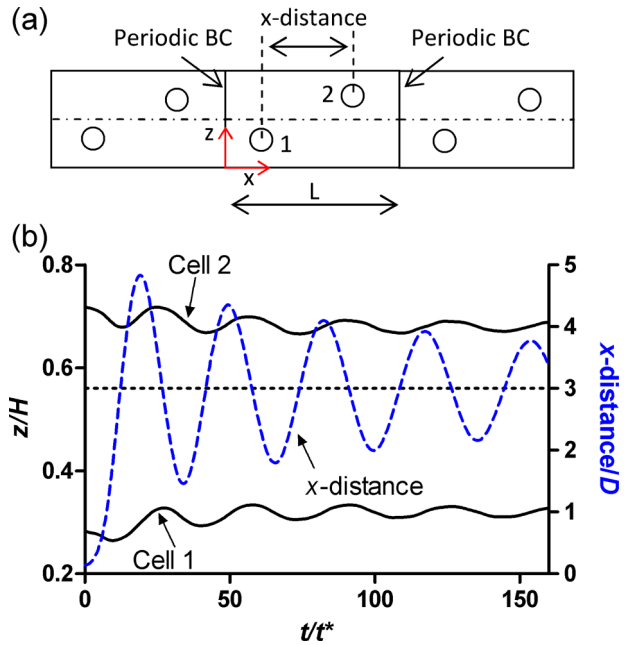

FIG. 7. (Color online) (a) Diagram of a long series of cells located in different halves of the channel. (b) Time evolution of the cell lateral positions (solid lines) and cell-to-cell x distance (blue dashed line) when z_0/H for cells 1 and 2 is 0.28 and 0.72, respectively. The channel length is $6D$, and the initial translational position x_0/H for cells 1 and 2 is 0.59 and 0.61, respectively. Re $= 10$, $\gamma = 10^4$, $D/H = 0.2$.

in the translational direction also oscillated with time around the average x distance [blue dashed line in Fig. 6(b)]. This oscillatory dynamics of cells occurs while the cells are dragged by bulk flow toward the outlet, i.e., two interacting cells behave as two beads attached to a string with a dashpot that regularly contracts and relaxes during its movement in shear flow. The oscillation of the cells in the translational direction was out of phase (at a phase shift of 90°) with the oscillation in the lateral direction, but the periods of these oscillations were the same. The maximum amplitude was $3.36D$, which was more significant than the amplitude of the lateral oscillation. After the decay of the oscillations, the cells reached the same lateral equilibrium position and the same x distance (half of the channel length) between them, in qualitative agreement with the experimental results of Lee *et al.* [49] on particle self-assembly in a microchannel. When the computational domain length decreased to six times the cell diameter, the period of the oscillations decreased to $30.6t^*$ and the maximum amplitude became $0.179D$. The oscillation period was proportional to the computational domain length because the rate of decrease in the domain length was always equal to the rate of the period decrease.

Our next short-channel simulation deals with two cells initially located in the top and bottom halves of the channel [Fig. 7(a)]. Here, the channel length was six times the cell diameter. The initial x distance between the cells was $0.14D$. As seen in Fig. 7(b), both cells experienced damped oscillations in both lateral and translational directions. During these in-phase (phase shift $= 0°$) oscillations with the maximum lateral amplitude of about $0.21D$, they were slowly drifting to their expected lateral equilibrium positions. These positions were symmetric around the centerline, i.e., if the bottom cell went to the equilibrium position z_{eq}, the top cell reached the equilibrium position $H-z_{eq}$. Cell 1 moved faster in the x direction than cell 2 because it was closer to the centerline. This resulted in an increase in the x distance with time until $t/t^* \approx 21$, when the x-distance-damped oscillation around the distance of three times the cell diameter began [blue dashed line in Fig. 7(b)]. The equilibrium x distance was half of the channel length, which indicates that the cells were evenly distributed along the translational direction.

Figure 8 shows the short-channel simulation data when two cells have very large initial z distance but are still located in the same half (bottom or top) of the channel. The upper cell repeatedly collided with the lower one. Similarly to Fig. 3(a), during every collision, the cells have opposite spikes in their lateral position. These repeated collisions kept them from reaching the single-cell equilibrium position. The spike height for the lower cell (cell 1) was shorter due to the wall repulsion. Eventually, due to higher spikes, cell 2 moved further and further from the trajectory of the single cell migration. It finally crossed the centerline and entered the other half of the channel. After this happened, cell 2 continued to oscillate with higher amplitude but lower frequency, and the oscillations of both cells became in phase, similar to what was shown in Fig. 7(b).

The effect of deformability on pairwise cell interaction and migration in a microchannel for a long series of cells is displayed in Fig. 9. In this simulation, the channel length was ten times the cell diameter. Cell 2 was more deformable than cell 1 and initially positioned closer to the centerline. This case was selected because more deformable cells generally have lateral equilibrium positions closer to the centerline [34]. As in Fig. 9,

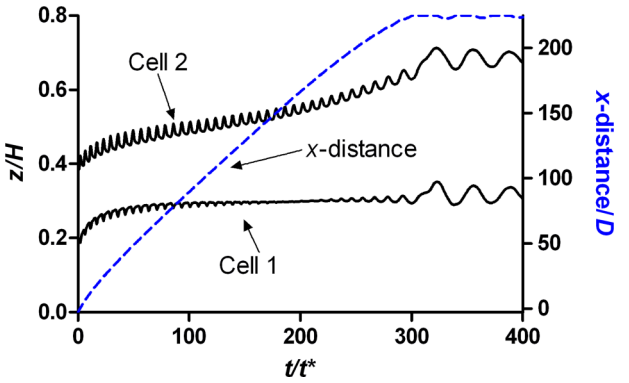

FIG. 8. (Color online) The migration of a series of identical periodically spaced cells (two lines of cells with a large initial z distance between them). The initial lateral position z_0/H for cells 1 and 2 is 0.186 and 0.386, respectively. The channel length is $6D$, and the initial translational position x_0/H for cells 1 and 2 is 0.9 and 0.3, respectively. Re $= 10$, $\gamma = 10^4$, $D/H = 0.2$.

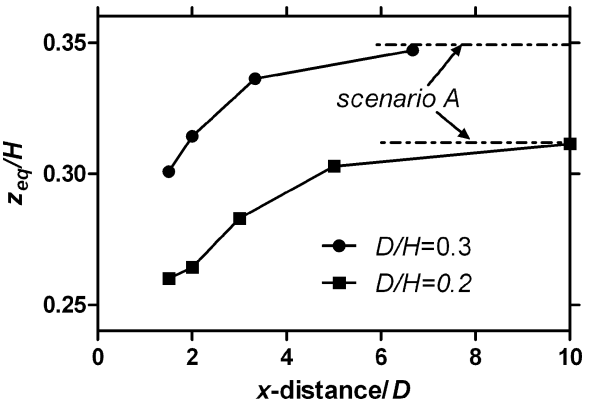

FIG. 10. Lateral equilibrium position of a series of identical periodically spaced cells as a function of x distance for different cell diameters. Dash-dot lines show the equilibrium position values according to scenario A (no interaction).

cell 2 collided and passed cell 1 repeatedly until reaching the equilibrium position closer to the centerline than cell 1. Cell 2 was unable to enter the top half of the channel, but the lateral distance between the cells increased significantly from the initial value. When compared to the scenario A simulation [34], this result indicates that the cell-cell interaction facilitates separation of cells with different deformability.

Finally, Fig. 10 shows the effect of the cell-cell separation distance on the lateral equilibrium position of a long series of cells migrating in the bottom half of the channel. In this case, the cells were equally spaced in the translational direction while having the same lateral position. The lateral equilibrium position becomes closer to the channel wall as the cell-cell separation distance shortens, in line with the computational work on Newtonian drops by Mortazavi *et al.* [71]. There was a strong interaction between the cells when the ratio of the x distance to the cell diameter was less than 5. The pairwise interaction effects were substantially weakened when the ratio became greater than 5, indicating that this value can serve as a threshold cell-to-cell distance for a transition from scenario AB to scenario A provided D/H is between 0.2 and 0.3. The difference in the lateral equilibrium position between *scenario A* [34] and the current simulation of scenario AB at the x distance of five times the cell diameter was less than 0.8%. Figure 10 also shows a decrease in the slope for smaller cells ($D/H = 0.2$) when the x distance decreases below $1.5D$. This effect is most likely caused by the wall repulsion that becomes higher as the cells get closer to the wall and by the close proximity of the cells.

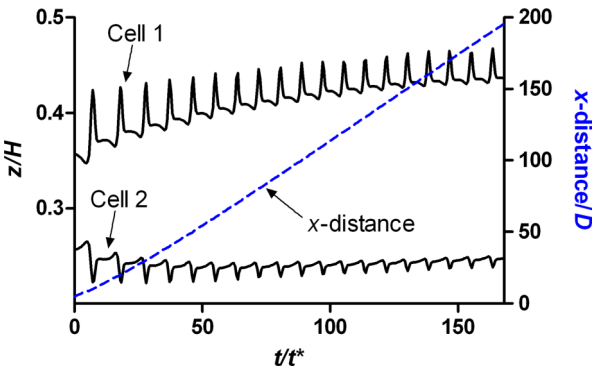

FIG. 9. (Color online) Time evolution of the lateral positions of two cells with different deformability. The initial lateral position z_0/H for cells 1 and 2 is 0.257 and 0.357, respectively. The channel length is $10D$, and the initial translational position x_0/H for cells 1 and 2 is 0.5 and 1.5, respectively. Re $= 10$, $\gamma_1 = 5 \times 10^4$, $\gamma_2 = 5 \times 10^3$, $D/H = 0.2$.

IV. CONCLUSIONS

In this computational study, we have investigated the effect of pairwise interaction of deformable cells on lateral and translational migration in a microchannel. When two identical cells are located in the bottom or top half of the channel at different lateral positions and not interacting with other cells, they pass each other or "bounce back" in the translational direction, eventually reaching the same lateral equilibrium position and large separation distance (more than ten times the cell diameter). The transient interaction between these cells leads to cell "swapping" in the lateral direction provided the lateral distance between the cells is small enough. "Swapping" can deleteriously influence cell separation or enrichment, likely putting the restriction on how small the channel length can be for these applications. Our study indicates that there is a threshold value in the lateral distance between the cells entering the channel for this phenomenon to occur. As the cell deformation increases, the threshold value becomes larger and the swapping has more chance to happen.

A series of identical cells closely spaced in the translational direction generally undergoes damped oscillation in both the lateral and translational directions until the cells reach equilibrium positions and become evenly distributed in the translational direction (self-assembly phenomenon). For a series of cells with different deformability, the cell-cell interaction leads to the migration of more deformable cells to the equilibrium position closer to the centerline, thereby facilitating cell separation.

ACKNOWLEDGMENTS

This work was supported by Louisiana Board of Regents Grant No. LEQSF(2011-14)-RD-A-24 and National Science Foundation Grant No. 13012861 (to D.K.), and the LONI Institute Graduate Fellowship and the Tulane-IBM Corporation Fellowship in Computational Science (to H.L.). We thank Dino Di Carlo and Wonhee Lee for helpful discussions.

[1] K. G. Phillips, A. Kolatkar, K. J. Rees, R. Rigg, D. Marrinucci, M. Luttgen, K. Bethel, P. Kuhn, and O. J. T. McCarty, Front. Oncol. **2**, 96 (2012).
[2] D. B. Khismatullin, Curr. Top. Membr. **64**, 47 (2009).
[3] H. L. Goldsmith and S. Spain, Microvasc. Res. **27**, 204 (1984).
[4] M. J. Pearson and H. H. Lipowsky, Am. J. Physiol.: Heart Circ. Physiol. **279**, H1460 (2000).
[5] G. W. Schmid-Schönbein, S. Usami, R. Skalak, and S. Chien, Microvasc. Res. **19**, 45 (1980).
[6] L. L. Munn, R. J. Melder, and R. K. Jain, Biophys. J. **71**, 466 (1996).
[7] B. Lincoln, H. M. Erickson, S. Schinkinger, F. Wottawah, D. Mitchell, S. Ulvick, C. Bilby, and J. Guck, Cytometry, Part A **59**, 203 (2004).
[8] H. Bow, I. V. Pivkin, M. Diez-Silva, S. J. Goldfless, M. Dao, J. C. Niles, S. Suresh, and J. Han, Lab Chip **11**, 1065 (2011).
[9] S. S. Shevkoplyas, T. Yoshida, L. L. Munn, and M. W. Bitensky, Anal. Chem. **77**, 933 (2005).
[10] H. Mohamed, M. Murray, J. N. Turner, and M. Caggana, J. Chromatogr. A **1216**, 8289 (2009).
[11] Z. Wu, B. Willing, J. Bjerketorp, J. K. Jansson, and K. Hjort, Lab Chip **9**, 1193 (2009).
[12] R. David, M. Groebner, and W. M. Franz, Stem Cells **23**, 477 (2005).
[13] A. A. Bhagat, H. Bow, H. W. Hou, S. J. Tan, J. Han, and C. T. Lim, Med. Biol. Eng. Comput. **48**, 999 (2010).
[14] A. J. Mach and D. Di Carlo, Biotechnol. Bioeng. **107**, 302 (2010).
[15] S. C. Hur, N. K. Henderson-MacLennan, E. R. B. McCabe, and D. Di Carlo, Lab Chip **11**, 912 (2011).
[16] D. Di Carlo, Lab Chip **9**, 3038 (2009).
[17] M. G. Lee, S. Choi, and J. K. Park, J. Chromatogr. A **1218**, 4138 (2011).
[18] M. Yamada, M. Nakashima, and M. Seki, Anal. Chem. **76**, 5465 (2004).
[19] H. Maenaka, M. Yamada, M. Yasuda, and M. Seki, Langmuir **24**, 4405 (2008).
[20] A. Karnis, H. L. Goldsmith, and S. G. Mason, Nature **200**, 159 (1963).
[21] S. Sukumaran and U. Seifert, Phys. Rev. E **64**, 011916 (2001).
[22] J. Magnaudet, S. Takagi, and D. Legendre, J. Fluid Mech. **476**, 115 (2003).
[23] M. Abkarian and A. Viallat, Biophys. J. **89**, 1055 (2005).
[24] B. Kaoui, G. H. Ristow, I. Cantat, C. Misbah, and W. Zimmermann, Phys. Rev. E **77**, 021903 (2008).
[25] G. Danker, P. M. Vlahovska, and C. Misbah, Phys. Rev. Lett. **102**, 148102 (2009).
[26] G. Coupier, B. Kaoui, T. Podgorski, and C. Misbah, Phys. Fluids **20**, 111702 (2008).
[27] M. J. Martinez and K. S. Udell, J. Fluid Mech. **210**, 565 (1990).
[28] H. Zhou and C. Pozrikidis, Phys. Fluids **6**, 80 (1994).
[29] C. Coulliette and C. Pozrikidis, J. Fluid Mech. **358**, 1 (1998).
[30] A. J. Griggs, A. Z. Zinchenko, and R. H. Davis, Int. J. Multiphase Flow **33**, 182 (2007).
[31] A. Nourbakhsh and S. Mortazavi, Iran. J. Sci. Technol. B **34**, 179 (2010).
[32] T. Inamuro and Y. Kataoka, Philos. Trans. R. Soc. A **369**, 2528 (2011).
[33] D. B. Khismatullin, Y. Renardy, and V. Cristini, Phys. Fluids **15**, 1351 (2003).
[34] H. Lan and D. B. Khismatullin, Int. J. Multiphase Flow **47**, 73 (2012).
[35] A. Kilimnik, W. B. Mao, and A. Alexeev, Phys. Fluids **23**, 123302 (2011).
[36] W. K. Purves, D. Sadava, G. H. Orians, and H. C. Heller, *Life: The Science of Biology* (Sinauer Associates, Sunderland, MA, 2004).
[37] H. Schmid-Schonbein, G. V. Born, P. D. Richardson, N. Cusack, H. Rieger, R. Forst, I. Rohling-Winkel, P. Blasberg, and A. Wehmeyer, Biorheology **18**, 415 (1981).
[38] D. A. Fedosov, J. Fornleitner, and G. Gompper, Phys. Rev. Lett. **108**, 028104 (2012).
[39] D. A. Fedosov, H. Noguchi, and G. Gompper, Biomech. Model. Mechanobiol. **13**, 239 (2014).
[40] R. Fahraeus, Physiol. Rev. **9**, 241 (1929).
[41] R. Zhao, M. V. Kameneva, and J. F. Antaki, Biorheology **44**, 161 (2007).
[42] M. M. Dupin, I. Halliday, C. M. Care, L. Alboul, and L. L. Munn, Phys. Rev. E **75**, 066707 (2007).
[43] C. Sun, C. Migliorini, and L. L. Munn, Biophys. J. **85**, 208 (2003).
[44] T. W. Pan, L. L. Shi, and R. Glowinski, Chin. Ann. Math. B **31**, 975 (2010).
[45] W. Wang, T. G. Diacovo, J. Chen, J. B. Freund, and M. R. King, PLoS One **8**, e76949 (2013).
[46] H. Zhao and E. S. G. Shaqfeh, Phys. Rev. E **83**, 061924 (2011).
[47] R. M. MacMeccan, J. R. Clausen, G. P. Neitzel, and C. K. Aidun, J. Fluid Mech. **618**, 13 (2009).
[48] L. L. Munn and M. M. Dupin, Ann. Biomed. Eng. **36**, 534 (2008).
[49] W. Lee, H. Amini, H. A. Stone, and D. Di Carlo, Proc. Natl. Acad. Sci. USA **107**, 22413 (2010).
[50] R. Tewhey, J. B. Warner, M. Nakano, B. Libby, M. Medkova, P. H. David, S. K. Kotsopoulos, M. L. Samuels, J. B. Hutchison, J. W. Larson, E. J. Topol, M. P. Weiner, O. Harismendy, J. Olson, D. R. Link, and K. A. Frazer, Nat. Biotechnol. **27**, 1025 (2009).
[51] Y. C. Tan and A. P. Lee, Lab Chip **5**, 1178 (2005).
[52] M. J. Fuerstman, P. Garstecki, and G. M. Whitesides, Science **315**, 828 (2007).

[53] J. Oakey, R. W. Applegate, E. Arellano, D. Di Carlo, S. W. Graves, and M. Toner, Anal. Chem. **82**, 3862 (2010).
[54] N. Pamme, Lab Chip **7**, 1644 (2007).
[55] D. Di Carlo, D. Irimia, R. G. Tompkins, and M. Toner, Proc. Natl. Acad. Sci. USA **104**, 18892 (2007).
[56] S. C. Hur, H. T. K. Tse, and D. Di Carlo, Lab Chip **10**, 274 (2010).
[57] K. J. Humphry, P. M. Kulkarni, D. A. Weitz, J. F. Morris, and H. A. Stone, Phys. Fluids **22**, 081703 (2010).
[58] M. Zurita-Gotor, J. Blawzdziewicz, and E. Wajnryb, J. Fluid Mech. **592**, 447 (2007).
[59] P. M. Kulkarni and J. F. Morris, J. Fluid Mech. **596**, 413 (2008).
[60] C. Migliorini, Y. Qian, H. Chen, E. B. Brown, R. K. Jain, and L. L. Munn, Biophys. J. **83**, 1834 (2002).
[61] D. R. Subramaniam, D. J. Gee, and M. R. King, J. Biomech. **46**, 1067 (2013).
[62] S. Jadhav, Y. C. Kit, K. Konstantopoulos, and C. D. Eggleton, J. Biomech. **40**, 2891 (2007).
[63] M. Loewenberg and E. J. Hinch, J. Fluid Mech. **338**, 299 (1997).
[64] E. Lac, A. Morel, and D. Barthès-Biesel, J. Fluid Mech. **573**, 149 (2007).
[65] K. Vahidkhah, S. L. Diamond, and P. Bagchi, Trans. ASME J. Biomech. Eng. **135**, 051002 (2013).
[66] D. B. Khismatullin and G. A. Truskey, Phys. Fluids **17**, 031505 (2005).
[67] D. Khismatullin, Y. Renardy, and M. Renardy, J. Non-Newtonian Fluid Mech. **140**, 120 (2006).
[68] J. U. Brackbill, D. B. Kothe, and C. Zemach, J. Comput. Phys. **100**, 335 (1992).
[69] G. W. Schmid-Schönbein, K. L. Sung, H. Tozeren, R. Skalak, and S. Chien, Biophys. J. **36**, 243 (1981).
[70] C. Dong, J. Cao, E. J. Struble, and H. H. Lipowsky, Ann. Biomed. Eng. **27**, 298 (1999).
[71] S. Mortazavi and G. Tryggvason, J. Fluid Mech. **411**, 325 (2000).